Journal of Sound and Vibration (1999) **228**(5), 961–975
Article No. jsvi.1999.2259, available online at http://www.idealibrary.com on IDEAL®

CREATING AND VERIFYING A RESEARCH-GRADE SIMPLY SUPPORTED CYLINDER WITH PZT ACTUATION

C. NIEZRECKI

Department of Mechanical Engineering, University of Florida, P.O. Box 116300, Gainesville, Florida 32611, USA

AND

H. H. CUDNEY

Department of Mechanical Engineering, Virginia Polytechnic Institute and State University, Blacksburg, VA 24061-0238, *USA*

(*Received* 12 *June* 1998, *and in final form* 15 *March* 1999)

In many aerospace and structural applications, idealized cylinders are used to approximate more complex structures such as airplane fuselages and rocket payload fairings. Many authors have created sophisticated models of the structural response of cylinders excited by a variety of actuators. However, these models are seldom verified experimentally. None of the models created to describe the response of a simply supported (SS) cylinder have ever been verified. In this work several different boundary conditions are created to approximate an ideal SS cylinder. The different boundary conditions tested are described and compared with finite-element analysis (FEA) and with an impedance-based analytical model for a piezoelectric actuator (PZT) exciting a SS cylinder. The work presented describes the steps taken in creating a physical boundary condition whichapproximates the ideal boundary condition for a SS cylinder and also evaluates the response of the impedance model for a PZT exciting a SS cylinder. The results indicate that the created physical boundary condition resembles the ideal SS boundary condition. The structural response computed by the impedance model is also shown to agree with the experiment and with the FEA. The results can be used to create other experimental SS cylinders and can also be used in modelling more complicated aerospace structures.

1. INTRODUCTION

Many aerospace and structural dynamics problems are too difficult to model analytically with exacting detail. To determine the general behavior of a distributed parameter system, researchers approximate complicated structures with simpler models such as beams, plates and cylinders. Idealized cylinders are used to approximate more complex structures such as airplane fuselages and rocket payload fairings [1, 2]. Previously, Arnold and Warburton performed some experiments on small diameter cylinders (97·8 mm diameter). They created a SS boundary condition by accurately machining a steel plate to fit the bore of the cylinder. The end-condition tolerance was found to be extremely critical in

0022-460X/99/500961 + 15 $30.00/0

obtaining results that are in fair agreement with the theory [3]. Sewall compared experiments on SS cylindrically curved panels with analysis. But no experiments on cylinders were performed [4]. Koga also studied the effects of boundary conditions on the free vibration of circular cylindrical shells. However, none of the boundary conditions he tested can be considered simply supported [5]. Presented in this paper are the steps taken in creating a physical boundary condition which approximates the ideal boundary condition for a SS cylinder. A variety of physical boundary conditions are tested and compared to determine the supports that most closely resemble the ideal SS conditions. The experimental results are compared to finite-element analysis FEA (using the software package I-DEAS) and to the analytical prediction based on Love's shell theory. A great deal of analytical work has been performed on the response of cylinders to a various excitation [6–10]. Many sophisticated and detailed models exist, however very rarely are these models ever verified through experiment. To the authors knowledge, the models created to describe the response of a simply supported (SS) cylinder have never been experimentally verified. The response of a SS cylinder excited by PZTs is also compared to an impedance-based model developed by Lalande [11, 12]. This work contributes to the knowledge base in two different ways. It represents the first time a SS cylinder has been readily constructed and whose dynamic properties are compared to analytical and finite-element analysis. Secondly, it represents the first time a model of a PZT actuator exciting a cylinder has been compared to experiment. Verification of the structural model will allow the cylinder's spatial response to be used in calculating the internal acoustic response and ultimately help to determine the feasibility of applying piezoelectric actuators to control rocket payload fairing vibrations and acoustics.

2. THEORETICAL DEVELOPMENT

The co-ordinate system used for the cylinder and actuator is shown in Figure 1. For a cylinder, the natural orthogonal modes can be used to determine the forced response using an infinite series

$$u_i(x, \theta, t) = \sum_{k=1}^{\infty} p_k(t)\, U_{ik}(x, \theta) e^{i\omega t}, \tag{1}$$

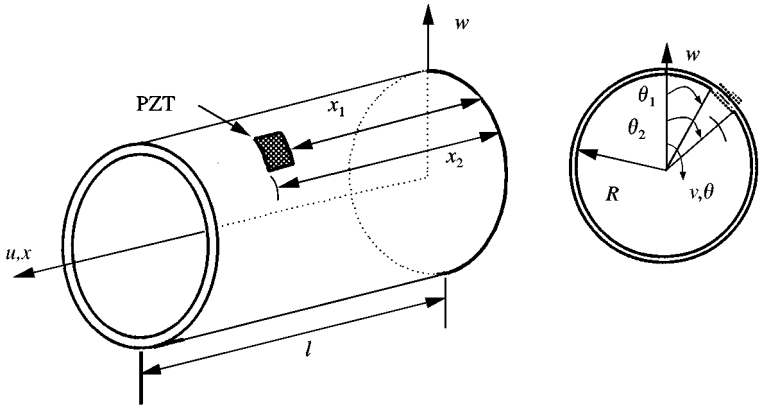

Figure 1. Cylinder with mounted actuators.

where the subscript i corresponds to the associated displacement (i.e. $i = 3$ represents transverse displacement), $p_k(t)$ represents the modal participation factor and $U_{ik}(x, \theta)$ is the spatial mode shape. For a SS cylinder the mode shape is given by [7]

$$U_{1k}(x, \theta) = A_{mnp}\cos(\alpha x)\cos(n\theta), \qquad U_{2k}(x, \theta) = B_{mnp}\sin(\alpha x)\sin(n\theta), \quad (2a, b)$$

$$U_{3k}(x, \theta) = C_{mnp}\sin(\alpha x)\cos(n\theta), \qquad \alpha = m\pi/L, \quad (2c, d)$$

where subscripts m and n represent the cylinder axial and circumferential modal index, respectively, and subscript p refers to one of the three principal co-ordinates (1, 2, 3). The equations that describe the motion of the cylinder are based on Love's equations for shell structures [7]. Previous models developed to compute the response of cylinders excited by PZTs are based on force inputs calculated at zero frequency excitation. Except for the impedance model, none of them take into consideration the changing impedance of the structure as a function of frequency. This will lead to an incorrect response if the structural impedance changes with frequency. The details of the impedance model to compute the structural response of the cylinder excited by piezoelectric actuators has been omitted for brevity and can be found in references [11, 12].

3. CREATION OF THE BOUNDARY CONDITION

The overall experimental setup used to model a SS cylinder is shown in Figure 2. The structure consists of an aluminum cylinder with several collocated PZT

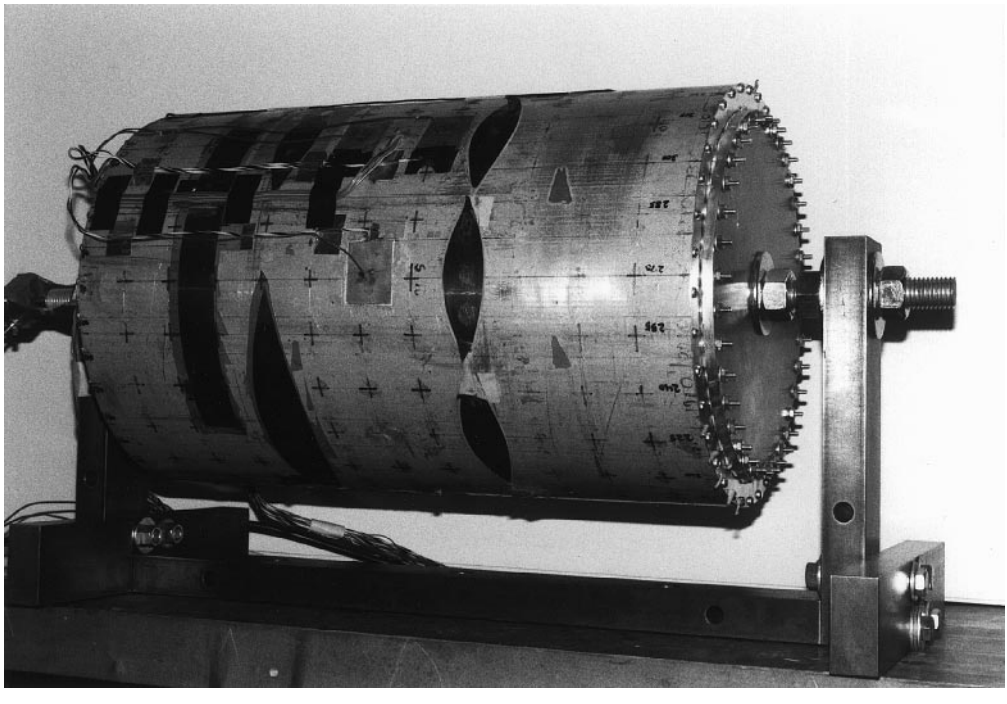

Figure 2. Instrumented cylinder.

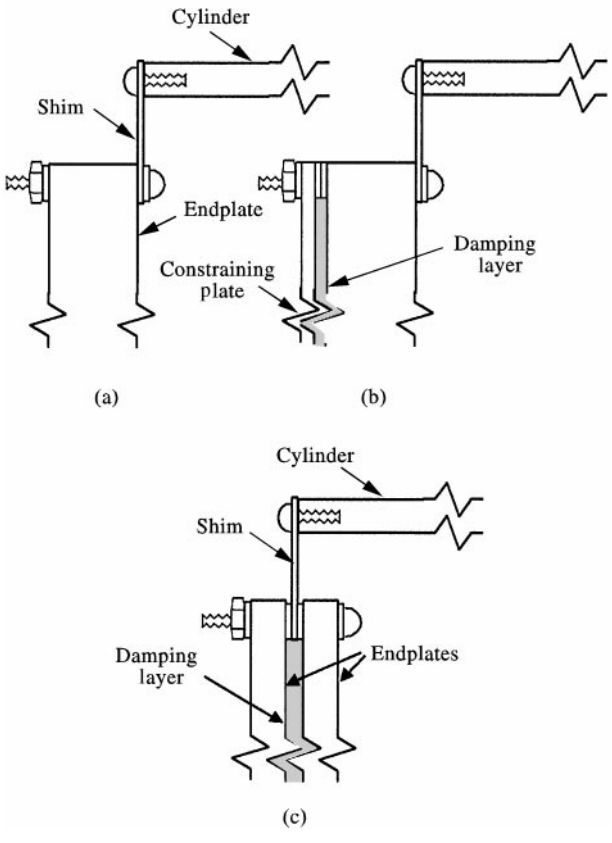

Figure 3. Tested boundary conditions: (a) test 1, 2, and 3; (b) test 4; (c) test 5.

actuators (G1195) attached at three different positions A, B, and C, driven in phase (A: $x = 0{\cdot}2032$ m, $\theta = 0°$; B: $x = 0{\cdot}1355$ m, $\theta = 0°$; C: $x = 0{\cdot}3048$ m, $\theta = 22{\cdot}5°$). The boundary conditions are created by using two thin aluminum annular shims (0·254 m outer diameter) and two or four aluminum endplates (0·2223 m diameter). The shims are screwed to the cylinder ends and bolted to the endplates (see Figure 3). Resin-dam vacuum sealant is used as a viscoelastic damping material when specified. The physical properties of the instrumented cylinder are described in Table 1. The purpose of the annular shim is to prevent the transverse motion of the cylinder at its two ends. This should be attainable since the membrane (in-plane) stiffness of the shim is very large. The shim is also kept thin so the bending moment introduced by the shim at the cylinder edges is very small. Since the bending stiffness is proportional to the cube of the thickness, for a plate, the stiffness of the cylinder should be several orders of magnitude larger than that of the shim. Likewise for the endplate, compared to the shim. To create a test stand that approximates a SS boundary condition, five different physical configurations were tested.

Test 1: For the first test, the annular shim (0·508 mm thick) is screwed to the ends of the cylinder and is attached to a 12·7 mm thick circular endplate (Figure 3(a)).

TABLE 1

Cylinder and actuator propeties

Property	Cylinder	PZT actuator
Young's modulus (Pa)	64×10^9	63×10^9
Density (Kg/m^3)	2700	7600
Poisson's ratio	0·3	0·3
Loss factor	0·005	0·001
Length (mm)	406·4	38·1
Diameter (mm)	254	—
Thickness (mm)	6·35	0·2413
Width (mm)	—	31·5
Applied voltage	—	50 or 25 Vr.m.s.
d_{32} (m/V)	—	-166×10^{-12}

Test 2: The setup is identical to Test 1 except a thinner annular shim (0·4064 mm) is used. This change was performed to see how altering the thickness (stiffness) of the shim affected the response.

Test 3: The setup is identical to Test 2 except the annular shim is now discontinuous and consists of 18 individual radially sliced, slotted segments. Each of the individual segments contains a radial slot 9·525 mm deep (0·762 mm wide) on the outer and inner edge located at the middle of the segment. This change was performed to reduce the coupling between the endplates and the cylinder.

Test 4: The setup is identical to Test 1 except a layer of damping material (2·08 mm) has been added along with a circular constraining aluminum plate (0·2223 m diameter, 1·588 mm thick). The plate is bolted outside of the cylinder onto the endplates. This change was designed to introduce some damping into the endplates and reduce their vibration (Figure 3(b)).

Test 5: The final setup used the same annular shim as in Test 1 except it is now being sandwiched in the middle between two 6·35 mm thick aluminum endplates (four in all). A layer of damping material (2·59 mm) separates the plates. This change was designed to center the shim at the natural axis of the endplate and so the high in-plane forces in the annular shim cannot excite the transverse displacement of the endplates. This change also placed the damping material in a region of maximum shear. The goal is to reduce the coupling between the endplates and the cylinder (Figure 3(c)).

4. SYNOPSIS OF BOUNDARY CONDITIONS TESTS

The displacement of the cylinder at $x = 0{\cdot}1016$ m, $\theta = 0^\circ$ (actuated by actuator B, 50 Vr.m.s.) for the five different boundary conditions can be seen in Figure 4. The circled region indicates where the largest interaction between the endplates and the cylinder occurs. This region corresponds to the second natural frequency of the circular endplate. The thinner shim from Test 2 is more strongly coupled than the

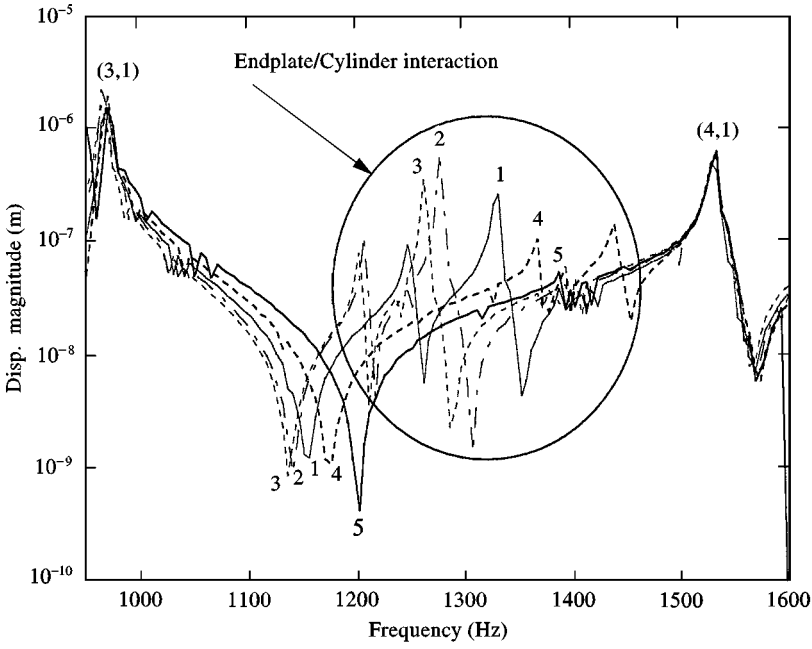

Figure 4. Response of the cylinder for different boundary conditions at $x = 4{\cdot}0$ in, $\theta = 0$: ——, test 1; – · –, test 2; - - -, test 3; – – –, test 4; ——, test 5.

0·508 mm shim from Test 1. It was expected that the slotted shim in Test 3 would decouple the endplate from the cylinder, however this was not found to be true. The effect of the slots was also found to increase the displacement at the ends of the cylinder. The fourth test implemented a constrained damping layer as shown in Figure 3(b). The damping layer did reduce endplate/cylinder interaction. The final test placed the shim at the neutral axis of the endplate and is denoted by the darkest of the five lines in Figure 4. Test five shows very little coupling between the cylinder and the endplate. Although not shown, Test 5 also resulted in the smallest edge displacements by far and an order of magnitude decrease in the vibration of the endplates for virtually all frequencies compared to any of the other tests. The remaining experiments are performed using the boundary conditions described for Test 5 (Figure 3(c)).

5. MODAL EVALUATION OF THE CYLINDER

To determine the modal properties of the cylinder a roving modal hammer test was performed. A Kistler 8620 accelerometer was used to measure the response ($x = 0{\cdot}359$ m, $\theta = 0°$) for various equally spaced axial ($x = 0, 33{\cdot}87, 67{\cdot}73, 101{\cdot}6, \ldots, 372{\cdot}5, 406{\cdot}4$ mm, $\theta = 0°$) and angular ($x = 67{\cdot}73$ and $237{\cdot}1$ mm, $\theta = 0, 10, 20, \ldots, 180°$) impact positions using a Kistler 9712A50 force transducer. Because of the reciprocity principle, the hammer was moved instead of the accelerometer. This produces equivalent results to a roving accelerometer test.

6. RESULTS OF THE MODAL TESTS AND FEA

The FRFs for half of the cylinder in the axial direction are shown in Figure 5 (hammer strikes at $x = 0, 33{\cdot}87, 67{\cdot}73, 101{\cdot}6, 135{\cdot}5, 169{\cdot}3, 203{\cdot}2$ mm, $\theta = 0^\circ$). Little can be learned from Figure 5 except for the location of the resonant frequencies. The modal indices (n, m: circumferential, axial) are placed next to the associated peak for clarity. To determine the dominant modal index at a particular frequency it is necessary to look at Figures 6–8. The axial modal index is determined from Figure 6 by observing the spatial displacement pattern at a particular frequency. It should be noticed that the displacements at the edges of the cylinder are very small compared to the displacement away from the edge. This is what is expected for a cylinder with SS boundary conditions. The circumferential modal index is determined by observing the displacement pattern for various angular positions at a given frequency. Since measurements were performed only on half of the cylinder, the results in the angular direction are mirrored about $\theta = 180^\circ$. Results are shown for only two frequencies, 950 Hz and 1838 Hz, due to space limitations (see Figures 7 and 8). From Figure 7 it is determined that the resonant frequency at 950 Hz corresponds to the (2,1) mode for the cylinder. Likewise, the resonant frequency at 1838 Hz corresponds to the (3,2) mode for the cylinder (see Figure 8).

A finite-element analysis was performed with the software I-DEAS using 30 axial and 72 circumferential thin shell elements. The natural frequencies of the analytical model (based on Love's equations), experimental natural frequencies, and frequencies predicted by FEA are shown in Table 2. The results are compared in Figure 9. The analytical and FEA natural frequencies have an overall relative difference of 1·32% for the 16 modes. The deviation between the analytical and

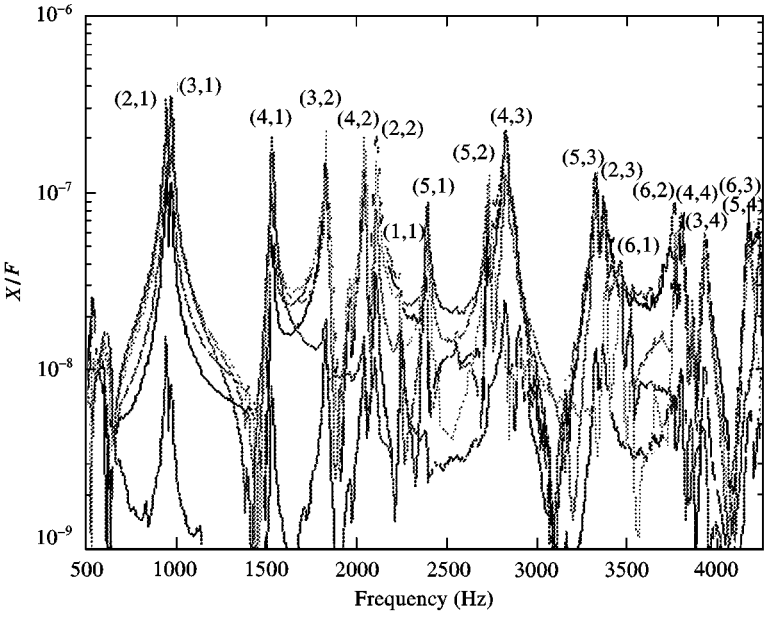

Figure 5. Response of the cylinder at different axial locations.

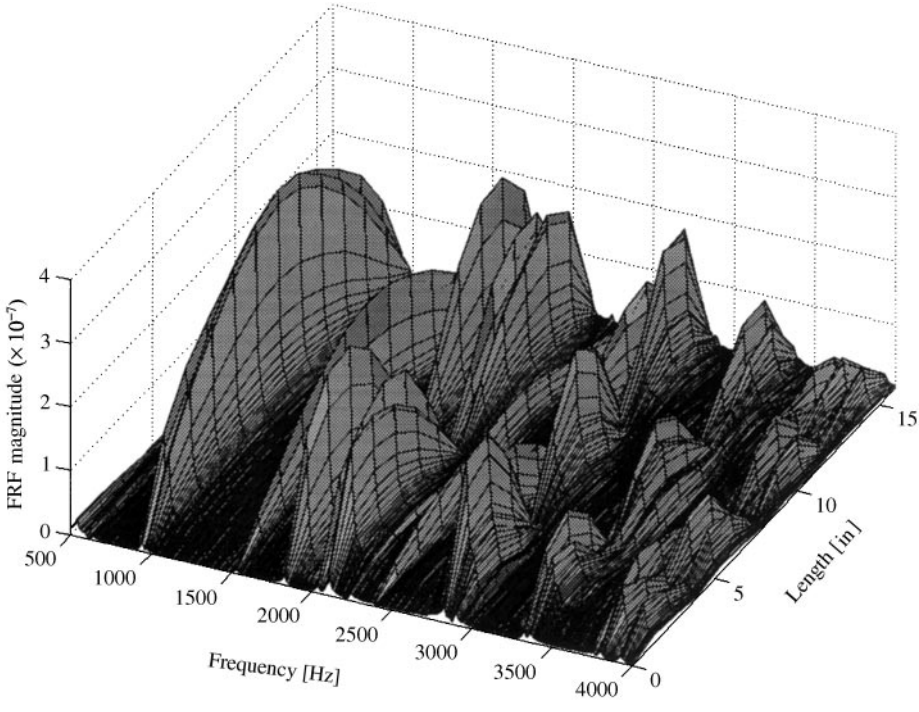

Figure 6. FRF of accelerance with respect to force.

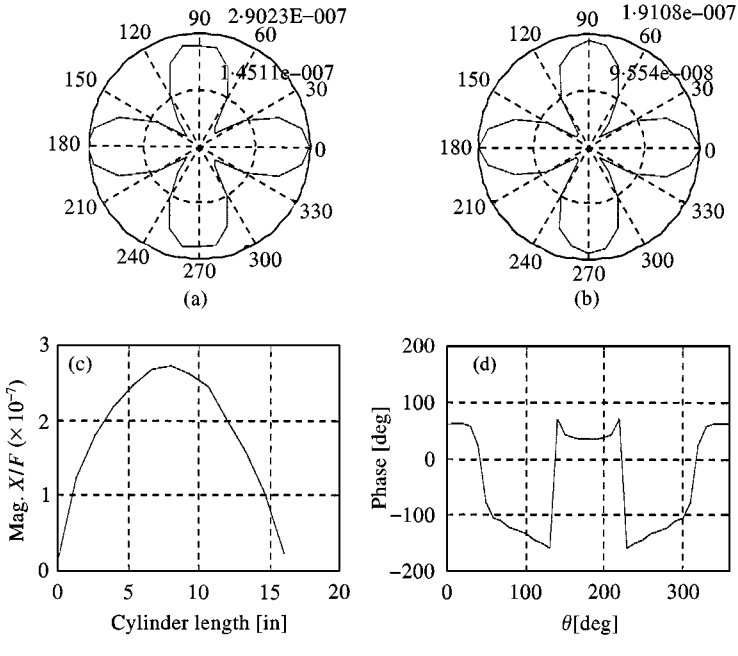

Figure 7. Spatial FRF magnitude at 950 Hz (2,1): (a) circumferential at $x = 237$ mm; (b) circumferential at $x = 67{\cdot}8$ mm; (c) axial at $\theta = 0°$; (d) circumferential phase at $x = 67{\cdot}8$ mm.

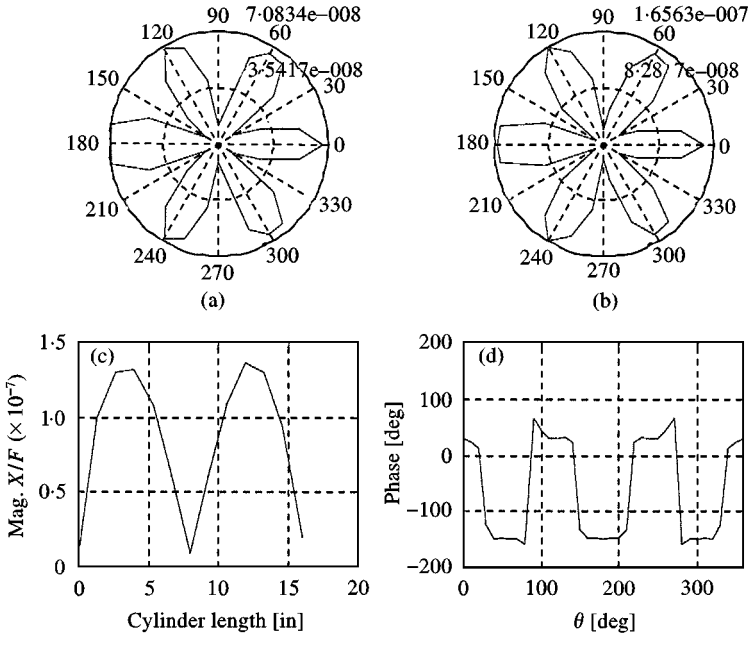

Figure 8. Spatial FRF at 1838 Hz (3,2): (a) circumferential at $x = 237$ mm; (b) circumferential at $x = 67{\cdot}8$ mm; (c) axial at $\theta = 0°$; (d) circumferential phase at $x = 67{\cdot}8$ mm.

TABLE 2

Cylinder analytical, FEA, and experimental natural frequencies

Mode	Analytical	FEA	Experimental
(3,1)	981 (Hz)	968	975
(2,1)	1084	1079	950
(4,1)	1530	1512	1538
(3,2)	2022	2000	1838
(4,2)	2082	2039	2044
(1,1)	2190	2189	2232
(5,1)	2378	2351	2395
(5,2)	2740	2679	2731
(2,2)	2798	2793	2113
(4,3)	3013	2950	2831
(3,3)	3251	3223	—
(5,3)	3420	3321	3337
(6,1)	3440	3397	3475
(6,2)	3739	3657	3760
(4,4)	4065	3983	3800
(2,3)	4153	4145	3363
(6,3)	4289	—	4233
(5,4)	4331	—	4168
(3,4)	4352	—	3925

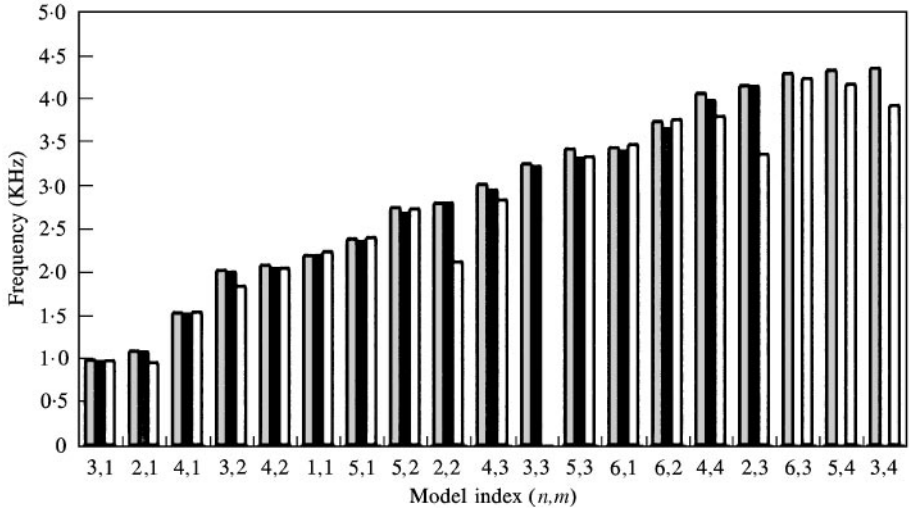

Figure 9. Comparison of analytical (▒), FFA (■), and experimental (□) natural frequencies.

experimental natural frequencies ranges from 0·5 to 24.5% depending on the mode. The major difference occurs in the two and three circumferential modes for the tested frequency range. It is believed that this deviation is caused because of the close proximity of the second (1200 Hz) and third (3850 Hz) modes of the endplate. In general, the analytical and experimental modes of the cylinder share the same modal order and are relatively close. The SS cylinder created to model an ideal SS cylinder is clearly not perfect. It does however have very similar vibrating properties and modal distribution.

7. RESPONSE TO VARIOUS ACTUATOR LOCATIONS

To help verify the response of the cylinder to excitation at different locations, the cylinder is excited at different positions and the response is compared (A: $x = 203{\cdot}2$ mm, $\theta = 0^\circ$; B: $x = 135{\cdot}5$ mm, $\theta = 0^\circ$; C: $x = 304{\cdot}8$ mm, $\theta = 22{\cdot}5^\circ$). Actuators A, B, and C are used to excite the cylinder at 25 Vr.m.s. using a sine-dwell test over a broad frequency range measured at $x = 338.7$ mm $\theta = 0^\circ$ for actuators A and B and $x = 67{\cdot}73$ mm, $\theta = 22{\cdot}5^\circ$ for actuator C. The analytical and experimental results are shown in Figures 10 and 11 respectively. For actuator A, the analytical model predicts the actuator will strongly excite the odd axial modes and ignore the even axial modes. This makes physical sense since actuator A is located at the center of the cylinder and is verified by Figure 11. For actuator B, the analytical model predicts the actuator will excite the odd axial modes and will ignore the three axial modes. Similar trends are seen in Figure 11. Lastly, the actuator located $\frac{1}{4}$ of the length of the cylinder, actuator C, is predicted to excite the axial two modes the most. This is also confirmed by the experiment. An exception to this general behavior occurs at the (6,2) mode where it is expected that actuator A should not produce any excitation. However, both the analysis and experiment

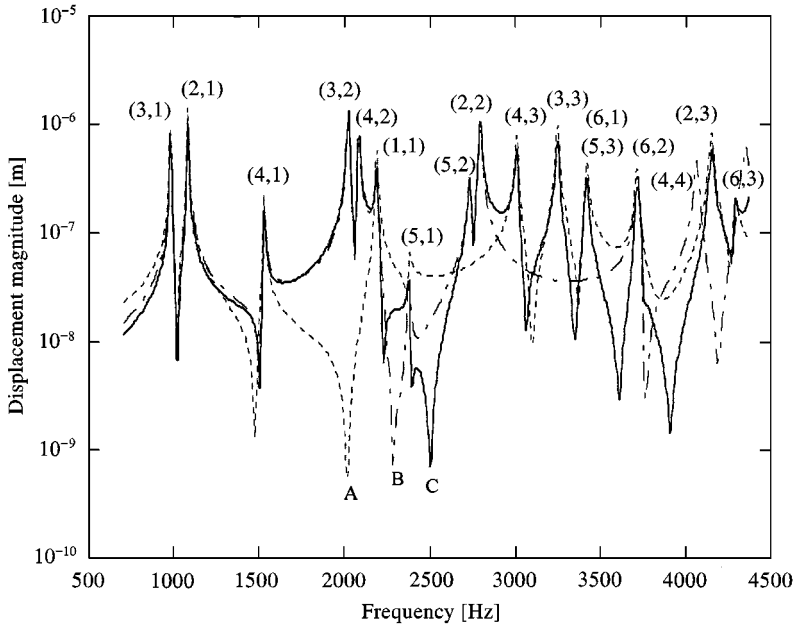

Figure 10. Analytical displacement magnitude, driven by different actuators: - - -, A; – · –, B; ——, C.

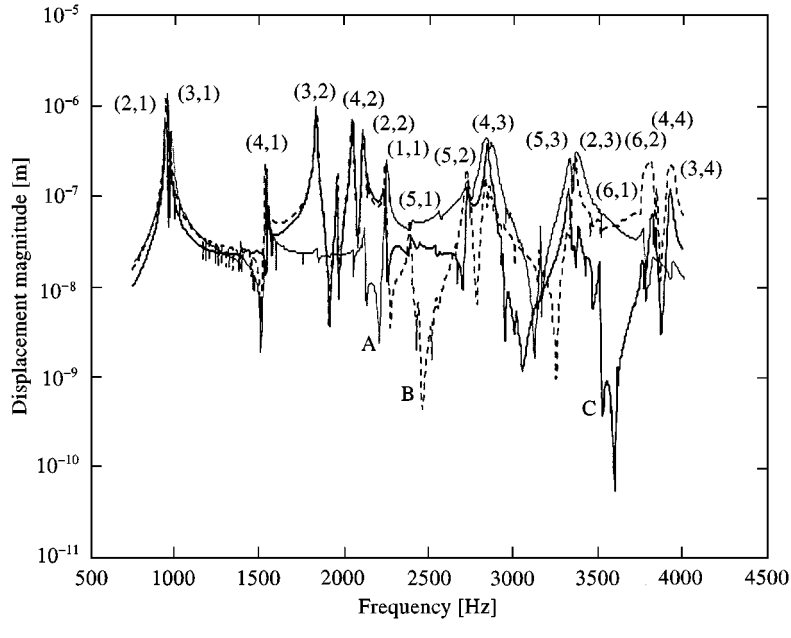

Figure 11. Experimental displacement magnitude driven by different actuators: - - -, A; – – –, B; ——, C.

show a strong coupling at the frequency. The overall analytical response follows the expected physical trends with respect to actuator location and is similar to the experimental results.

8. ANALYTICAL AND EXPERIMENTAL RESPONSE

Presented in Figures 12 and 13 are the analytical and experimental response of the cylinder for actuator A and B measured at $x = 338{\cdot}7$ mm, $\theta = 0°$. The relative

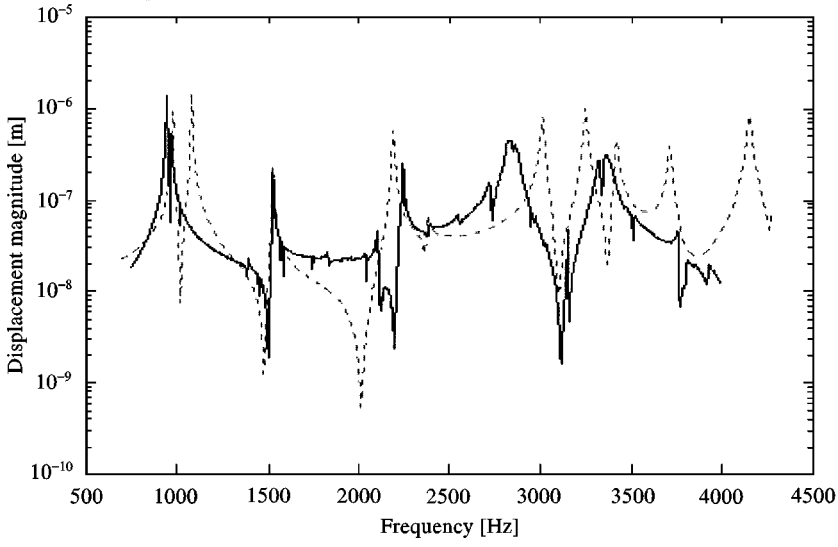

Figure 12. Analytical/experimental displacement magnitude at $x = 13{\cdot}33$ in, $\theta = 0$ for PZT A at 25 Vr.m.s: - - -, analytical; ——, experimental.

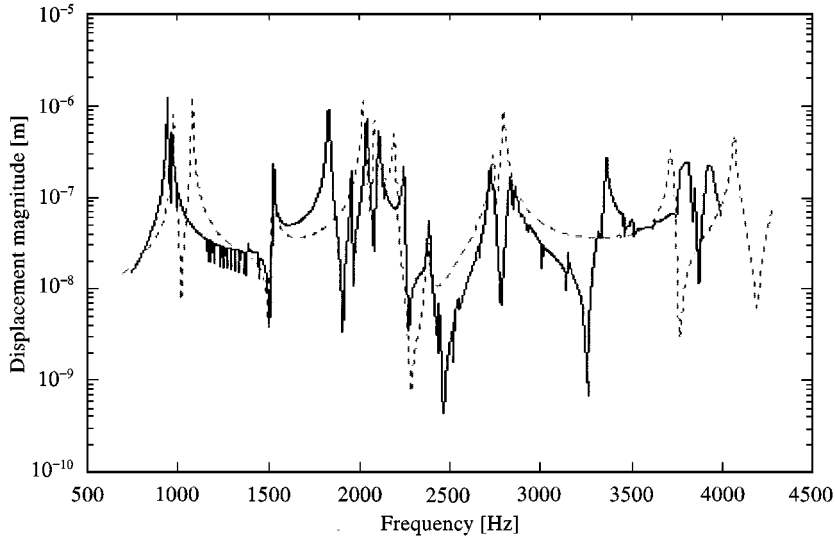

Figure 13. Analytical/experimental displacement magnitude at $x = 13{\cdot}33$ in, $\theta = 0$ for PZT B at 25 Vr.m.s: - - -, analytical; ——, experimental.

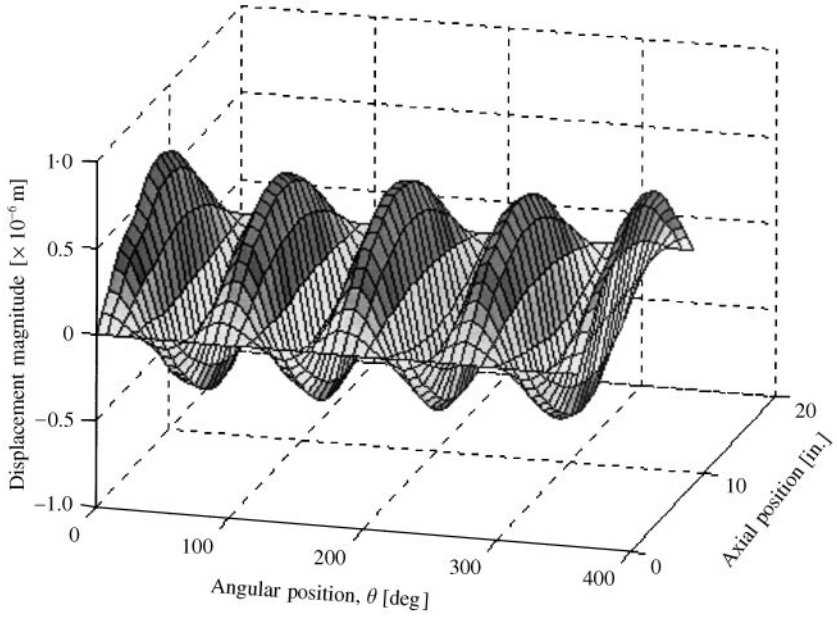

Figure 14. Analytical response at 1533 Hz (4,1).

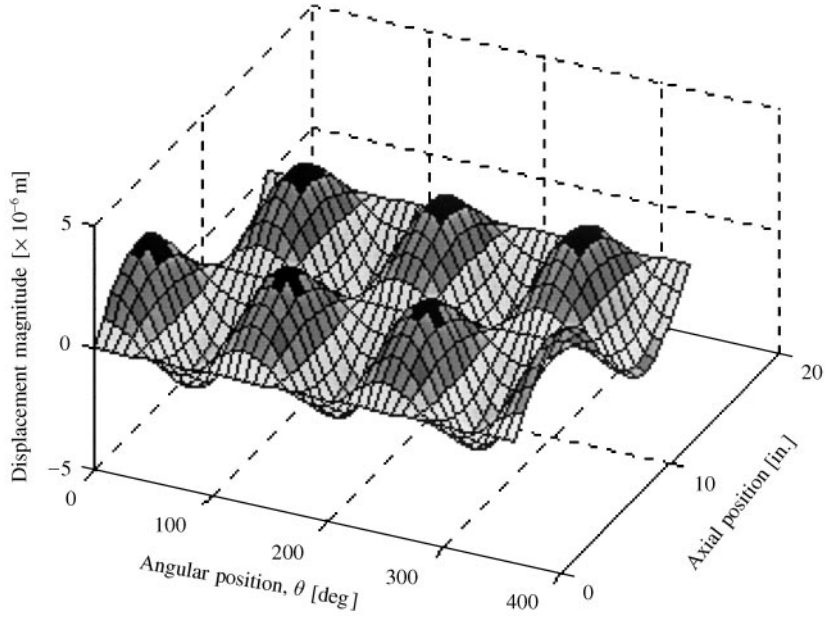

Figure 15. Analytical response at 2021 Hz (3,2).

magnitude of the predicted response is similar to the measured response using an overall structural damping value of 0·5% (the predicted response magnitude depends on the damping value). Even though the frequencies of some modes are shifted, the dominant behavior of the cylinder is predicted by the model.

For the analytical natural frequencies, which correspond to the (4,1) and (3,2) modes, the analytical spatial displacement response is shown in Figures 14 and 15. The phase of the displacement response has been incorporated into the plots to show actual normal displacements. As is expected for each of these frequencies, the predicted operating shape is similar to the dominant mode. The results indicate that the impedance model for PZTs actuating a SS cylinder can approximate the overall resonant and modal behavior.

9. CONCLUSIONS

The work presented describes the steps taken in creating a physical boundary condition which approximates the ideal boundary condition for a SS cylinder. The results indicate that the created physical boundary condition resembles the ideal SS boundary condition but is not perfect. It does however have very similar vibrating properties and modal distribution. The analytical model predicts the expected physical changes to the response as the actuator location is shifted. The structural response computed by the impedance model is also shown to be similar to the experimental response and matches the natural frequencies determined using FEA. The results can be used to create other experimental SS cylinders and can also be used in modelling more complicated aerospace structures.

ACKNOWLEDGMENTS

This work is sponsored by the Air Force Office of Scientific Research grant #'s F49620-93-1-0280 and by F49620-94-1-0346 through the Center for Optimal Design and Control at VPI&SU. Thanks are given to Dr. Marc Jacobs (contract monitor), Dr. Alok Das and Capt. Jeanne Sullivan (Phillips Laboratory).

REFERENCES

1. C. NIEZRECKI and H. H. CUDNEY 1997 *Proceedings of the AIAA/ASME/ASCE/AJS/ASC 38th Structures, Structural Dynamics, and Materials Conference, Adaptive Structures Forum, Kissimmee, FL*, 1525–1535. Active control technology applied to rocket fairing structural vibrations and acoustics.
2. H. C. LESTER and S. LEFEBVRE 1991 *Proceedings, Recent Advances in Active Noise and Vibration Control, Blacksburg, VA, Technomic Publishing Company, Inc., April* 15–57, 3–26. Piezoelectric actuator model for active sound and vibration control of cylinders.
3. R. N. ARNOLD and G. B. WARBURTON 1949 *Proceedings of the Royal Society of London, Series A*, **197**, 238–256. Flexural vibrations of the walls of thin cylindrical shells having freely supported ends.
4. J. L. SEWALL 1967 *NASA TN D*-3791, *N*67-16689, 1–48. Vibration analysis of cylindrically curved panels with simply supported or clamped edges and comparison with some experiments.
5. T. KOGA 1988 *AIAA Journal* **26**, 1387–1394. Effects of boundary conditions on the free vibrations of circular cylindrical shells.
6. L. CHENG 1994 *Journal of Sound and Vibration* **174**, 641–654. Fluid–structural coupling of a plate-ended cylindrical shell: vibration and internal sound field.
7. W. SOEDEL 1981 *Vibrations of Shells and Plates*. New York: Marcel Dekker, Inc.

8. V. R. Sonti and J. D. Jones 1991 *Proceedings, Recent Advances in Active Noise and Vibration Control, Blacksburg, VA, Technomic Publishing Company, Inc.*, 3–26, April 15–17, 27–38. Active vibration control of thin cylindrical shells using piezo-electric actuators.
9. H. T. Banks, H. C. Lester and R. C. Smith 1992 *Proceedings of* 31*st Conference on Decision and Control, Tuscon, Arizona, December*, 1797–1802. A piezoelectric actuator model for active vibration and noise control is thin cylindrical shells.
10. V. R. Sonti and J. D. Jones 1996 *AIAA Journal* **34**, 1034–1040. Curved piezoelectric model for active vibration control of cylindrical shells.
11. F. Lalande, Z. Chaudhry and C. A. Rogers 1995 *Journal of Intelligent Material Systems and Structures* **6**, 389–395. Impedance based modeling of actuators bonded to shell structures.
12. F. Lalande 1995 *Ph.D. Dissertation, Virginia Polytechnic Institute and State University*. Modeling of induced strain actuation of shell structures.

NOMENCLATURE

u, x	axial co-ordinate
θ	angular co-ordinate
L	cylinder length
R	cylinder radius
t	time
U	cylinder mode shape
ω	angular frequency
p_k	modal co-ordinate
m, n	cylinder axial and circumferential modal indices
A, B, C	mode shape constants